

# How the headpiece hinge angle is opened: new insights into the dynamics of integrin activation

Eileen Puklin-Faucher,<sup>1,2</sup> Mu Gao,<sup>3,4</sup> Klaus Schulten,<sup>3,4</sup> and Viola Vogel<sup>1</sup>

<sup>1</sup>Department of Materials, Swiss Federal Institute of Technology in Zurich (ETH Zurich), CH-8093 Zurich, Switzerland

<sup>2</sup>Department of Chemistry, University of Washington, Seattle, Washington 98195

<sup>3</sup>Beckman Institute and <sup>4</sup>Department of Physics, University of Illinois at Urbana-Champaign, Urbana, Illinois 61801

**H**ow the integrin head transitions to the high-affinity conformation is debated. Although experiments link activation with the opening of the hinge angle between the  $\beta$ A and hybrid domains in the ligand-binding headpiece, this hinge is closed in the liganded  $\alpha_v\beta_3$  integrin crystal structure. We replaced the RGD peptide ligand of this structure with the 10th type III fibronectin module ( $\text{FnIII}_{10}$ ) and discovered through molecular dynamics (MD) equilibrations that when the conformational constraints of the leg domains are lifted, the  $\beta$ A/hybrid hinge opens

spontaneously. Together with additional equilibrations on the same nanosecond timescale in which small structural variations impeded hinge-angle opening, these simulations allowed us to identify the allosteric pathway along which ligand-induced strain propagates via elastic distortions of the  $\alpha 1$  helix to the  $\beta$ A/hybrid domain hinge. Finally, we show with steered MD how force accelerates hinge-angle opening along the same allosteric pathway. Together with available experimental data, these predictions provide a novel framework for understanding integrin activation.

## Introduction

The interplay of mechanical forces between cells and their surroundings regulates crucial processes such as cell shape, differentiation, and protein expression (Bershadsky et al., 2003; Ingber, 2003; Katsumi et al., 2004; Vogel and Sheetz, 2006). Integrins are large transmembrane adhesion proteins that provide the physical link between the extracellular matrix and the contractile cytoskeleton. Integrins are heterodimers, composed of  $\alpha$  and  $\beta$  subunits that associate noncovalently to form an extracellular, ligand-binding headpiece, followed by two multi-domain “legs,” two transmembrane helices, and two cytoplasmic tails (Fig. 1 A).

Integrins are not constitutively active. Rather, ligand-binding affinity is regulated via conformational change that can originate from cytoplasmic or extracellular interactions (Hynes, 2002). For example, ligand binding has been shown to induce the opening of the hinge angle between the  $\beta$ A (also called the I-like or  $\beta$ I domain) and hybrid domains in the integrin headpiece (Takagi et al., 2002, 2003; Mould et al., 2003b). Opening of this hinge has been linked to the switch to high

binding affinity (Luo et al., 2003, 2004b; Mould et al., 2003b). The x-ray crystallographic structures of the unliganded  $\alpha_v\beta_3$  and the liganded  $\alpha_{IIb}\beta_3$  integrins display the integrin headpiece conformations before and after the ligand-induced transition from the closed to the open  $\beta$ A/hybrid domain hinge, respectively (Xiong et al., 2001; Xiao et al., 2004). The  $\alpha 1$  and  $\alpha 7$  helices of the  $\beta$ A domain are known to be involved in this transition (Mould et al., 2002, 2003b; Yang et al., 2004).

Because of a lack of dynamic, nonequilibrium information, the sequential details by which structural change in the ligand-binding pocket is allosterically coupled to the remote hinge conformation at the  $\beta$ A/hybrid interface have remained unknown, as have the details of force-induced integrin conformational change, which would enable insights into how integrin function is kinetically regulated during cellular mechanosensing. With no techniques currently available to gain these details experimentally, we used MD and steered MD (SMD) to derive high-resolution, dynamic structural models computationally.

Our simulations are based on the liganded crystal structure of the  $\alpha_v\beta_3$  integrin, which was obtained by soaking RGD peptide into unliganded integrin crystals that were preformed with bent legs and a closed  $\beta$ A/hybrid hinge (Xiong et al., 2002). Although comparison of this crystal structure with the unliganded  $\alpha_v\beta_3$  integrin structure reveals ligand-induced conformational changes local to the binding site (Fig. S1, available at <http://www.jcb.org/cgi/content/full/jcb.200602071/DC1>), both

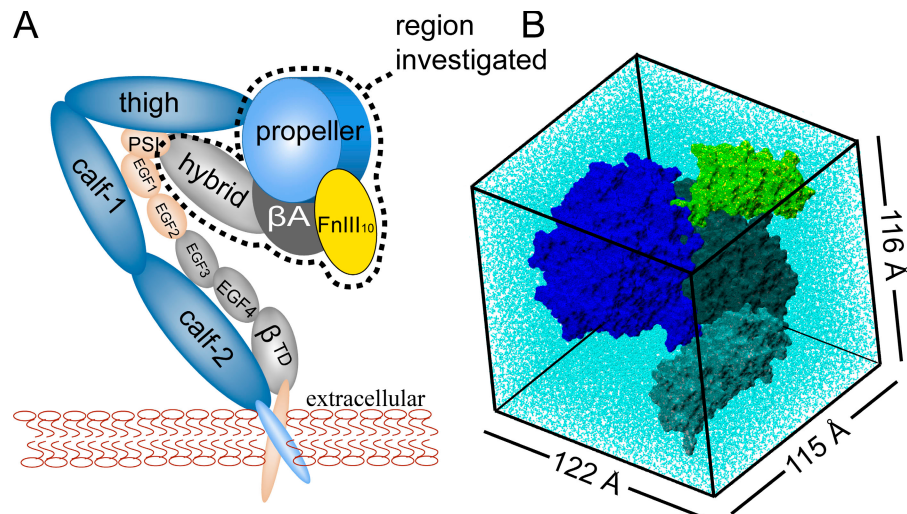
Correspondence to Viola Vogel: [viola.vogel@mat.ethz.ch](mailto:viola.vogel@mat.ethz.ch)

M. Gao's present address is the Center for the Study of Systems Biology, School of Biology, Georgia Institute of Technology, Atlanta, GA.

Abbreviations used in this paper: ADMIDAS, adjacent to the MIDAS; LIMBS, ligand-induced metal-binding site; MIDAS, metal ion-dependent adhesion site; MD, molecular dynamics; SMD, steered molecular dynamics.

The online version of this article contains supplemental material.

**Figure 1. Set up.** (A) Diagram of the FnIII<sub>10</sub> crystal structure (yellow; Leahy et al., 1996) docked to the liganded  $\alpha_v\beta_3$  integrin crystal structure (Xiong et al., 2002).  $\alpha$  and  $\beta$  subunits are indicated in blue and gray, respectively. Transmembrane domains and extracellular  $\beta$ -subunit domains not resolved in the original crystal structure were added in pink. (B) The FnIII<sub>10</sub>- $\alpha_v\beta_3$  integrin headpiece complex (908 residues) was simulated in a box of explicit water molecules.



structures share the same long-range conformation of bent legs and a closed  $\beta$ A/hybrid hinge. Thus, although unequivocally recognized as a milestone in integrin research, the liganded  $\alpha_v\beta_3$  integrin crystal structure has sparked much debate; does it represent the final, high-affinity conformation (Calzada et al., 2002; Xiong et al., 2003; Adair et al., 2005), or were the long-range, ligand-induced structural changes that underlie integrin activation arrested by conformational constraints (Takagi et al., 2002; Mould et al., 2003b, 2005; Xiao et al., 2004; Iwasaki et al., 2005)?

RGD ligands bind to the integrin  $\beta$  subunit via a divalent metal ion located at the top of the  $\beta$ A domain, termed the “metal ion-dependent adhesion site” (MIDAS; Xiong et al., 2002). Two additional ion-binding sites border the  $\beta$ A domain MIDAS on either side, which are termed the “ligand-induced metal-binding site” (LIMBS) and the “adjacent to the MIDAS” (ADMIDAS; Xiong et al., 2002). Although all three sites are occupied by ions when the ligand is bound (Xiong et al., 2002; Xiao et al., 2004), only the ADMIDAS is occupied in unliganded  $\alpha_v\beta_3$  crystal structures (Xiong et al., 2001, 2002). Moreover, the ADMIDAS of unliganded  $\alpha_v\beta_3$  crystal structures directly contacts the  $\beta$ 6- $\alpha$ 7 loop (Met<sup>335</sup>), whereas this contact is lost and the ADMIDAS is shifted inward by ~4 Å in both liganded  $\beta$ <sub>3</sub> integrin crystal structures (Xiong et al., 2001, 2002; Xiao et al., 2004).

Because integrins in a cellular context bind to extracellular matrix proteins, we replaced the RGD peptide in the liganded  $\alpha_v\beta_3$  integrin crystal structure (Xiong et al., 2002) with the RGD-containing 10<sup>th</sup> type III fibronectin (FnIII<sub>10</sub>) module (Leahy et al., 1996) and equilibrated this complex in a box of explicit water molecules and in the absence of the integrin legs. Domains included were the propeller domain from the  $\alpha$  subunit and the  $\beta$ A and hybrid domains from the  $\beta$  subunit (Fig. 1, A and B). Based on these simulations, together with equilibrations of the same domains from the unliganded  $\alpha_v\beta_3$  integrin crystal structure (Xiong et al., 2001), we propose that the energy barrier to ligand-induced hinge opening in the  $\alpha_v\beta_3$  headpiece is lowered by (a) the MIDAS conformation found in liganded crystal structures (Xiong et al., 2002; Xiao et al., 2004),

(b) Mg<sup>2+</sup> in place of Ca<sup>2+</sup> at the LIMBS and ADMIDAS, or (c) a stabilizing contact outside of the RGD-binding pocket between the top of the  $\alpha$ 1 helix and FnIII<sub>10</sub>, which is reported for the first time in this study. Finally, we show how ligand-mediated mechanical force accelerates hinge opening along the same allosteric pathway. Through comparison with current experimental data, we propose a structural model that provides new insight into existing notions of integrin activation.

## Results

Docking was performed without any major steric clashes by fitting the RGD loop of FnIII<sub>10</sub> (Leahy et al., 1996), which is known to be flexible (Copie et al., 1998), to the conformation of the RGD sequence in the liganded  $\alpha_v\beta_3$  crystal structure (Fig. 2 C; Xiong et al., 2002). The solvated FnIII<sub>10</sub>- $\alpha_v\beta_3$  integrin complex (Fig. 1 B) was investigated in 16 separate simulations of at least 6 ns each, consisting of 7 equilibrations (regular MD) and 9 simulations in which mechanical force was applied to an equilibrated complex (SMD). In the latter case, tensile stress was applied with a spring attached to the C or N terminus of FnIII<sub>10</sub> and pulled at a constant velocity. Because Mg<sup>2+</sup> ions are known to regulate integrin activation (Mould et al., 1995) and are present in the integrin under physiological conditions, all integrin metal ion-binding sites were occupied with Mg<sup>2+</sup>, unless specified otherwise. In all figures, FnIII<sub>10</sub> is yellow and the  $\beta$  subunit domains are colored according to the time point of the particular structural snapshot, with gray and black representing the starting conformations of the liganded and unliganded  $\alpha_v\beta_3$  crystal structures, respectively.

### The $\beta$ A/hybrid domain hinge opens spontaneously in the isolated FnIII<sub>10</sub>- $\alpha_v\beta_3$ integrin complex

A hydrogen bond between Asn<sup>303</sup> on the  $\beta$ A domain and Lys<sup>417</sup> on the hybrid domain, located where the closed hinge is most acute (Fig. 2 B), was permanently disrupted after 2.5 ns. Sequence analysis reveals that this Asn is completely conserved across the eight known integrin  $\beta$  subunits, whereas the Lys is

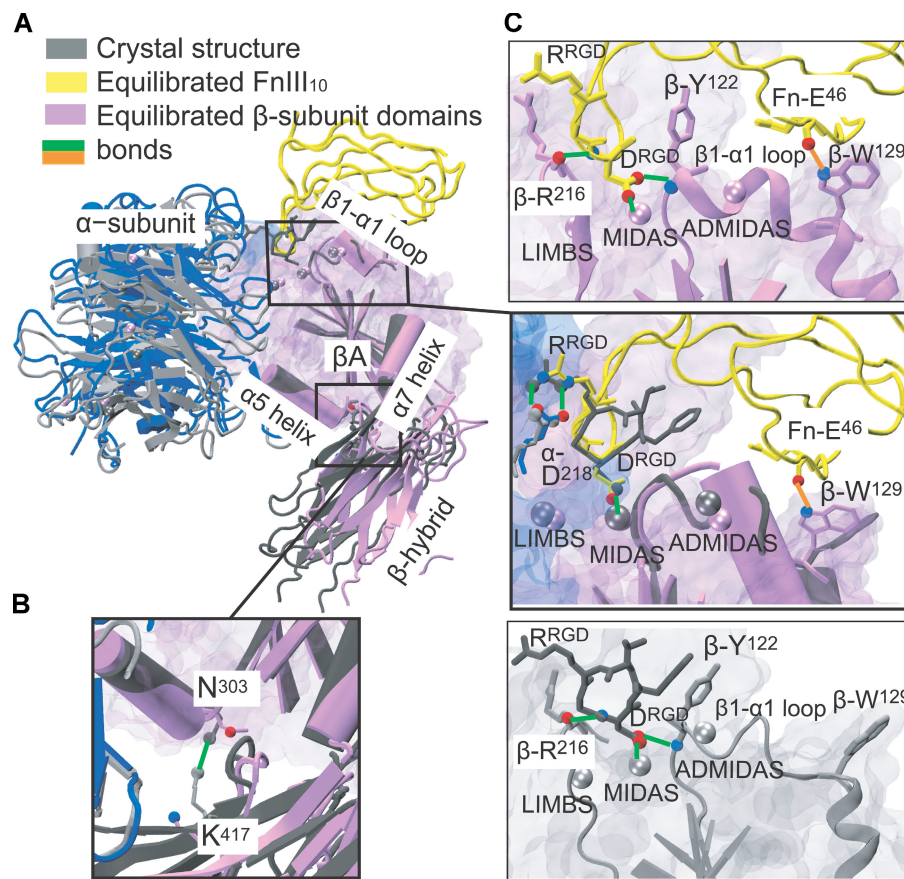


**Figure 2. Integrin headpiece hinge opening and receptor-ligand contact stability during MD equilibration.** (A) After 6 ns of MD, the equilibrated integrin complex (blue, purple, and yellow) is aligned with the starting crystal structure (gray; Xiong et al., 2002) via  $\beta$ A domain  $\beta$ -strands. For clarity, the  $\beta$ A domain is shown in transparent surface representation with the secondary structure of select regions visible in cartoon representation. (B) A close-up of the  $\beta$ A/hybrid domain interface shows the location inside the hinge of the hydrogen bond between Asn<sup>303</sup> and Lys<sup>417</sup>. This equilibrated complex, in which the Asn<sup>303</sup>–Lys<sup>417</sup> bond broke when the hinge spontaneously increased by  $\sim 20^\circ$ , is referred to in the text as the “reference complex.” (C, middle) In all of the equilibrated FnIII<sub>10</sub>–integrin complexes we investigated, independent of structural variations, the RGD loop of FnIII<sub>10</sub> (yellow) displayed close alignment with the conformation of the RGD sequence found in the original crystal structure (gray), and the two principle RGD–integrin binding contacts (Asp<sup>RGD</sup>–MIDAS ion and Arg<sup>RGD</sup>– $\alpha$ -Asp<sup>218</sup>) remained stable. (C, top and bottom). In the same, but separate, views of the equilibrated complex (top) and the liganded crystal structure (bottom), two additional Asp<sup>RGD</sup>– $\beta$ A domain-binding contacts that have been shown by pharmacophore refinement to be vital to the RGD– $\alpha$ , $\beta$ <sub>3</sub> ligand–integrin recognition process (Marinelli et al., 2003) displayed stability. These are hydrogen bonds between Asp<sup>RGD</sup>– $\beta$ -Arg<sup>216</sup> and Asp<sup>RGD</sup>– $\beta$ -Tyr<sup>122</sup>. Bonds present in the original crystal structure complex are shown in green. Also visible is a hydrogen bond between Fn-Glu<sup>62</sup> and  $\beta$ -Tyr<sup>129</sup> (orange) that formed in the equilibrated complex and was found to promote hinge angle opening on the nanosecond time frame.

conserved in four integrin  $\beta$  subunits ( $\beta_3$ ,  $\beta_4$ ,  $\beta_6$ , and  $\beta_8$ ) and is replaced by the similarly basic Arg in the other four  $\beta$  subunits ( $\beta_1$ ,  $\beta_2$ ,  $\beta_5$ , and  $\beta_7$ ). Once this bond was lost, the  $\beta$ A/hybrid domain hinge angle increased to an average of  $\sim 20^\circ$  greater than its value in the starting crystal structure for the remainder of the 7-ns equilibration (Fig. 3 C and Videos 1 and 2, available at <http://www.jcb.org/cgi/content/full/jcb.200602071/DC1>). We shall refer to this FnIII<sub>10</sub>– $\alpha$ , $\beta_3$  integrin complex as the “reference” complex, to distinguish it from additional complexes described in the article, in which the effect of various structural perturbations on spontaneous hinge opening was investigated.

In all complexes we investigated, ligand–receptor contacts that have been identified as vital to RGD– $\alpha$ , $\beta_3$  integrin–binding remained stable during equilibration (Fig. 2 C). In addition, a hydrogen bond consistently formed outside of the RGD-binding pocket, at a location between FnIII<sub>10</sub> and Trp<sup>129</sup> at the top of the  $\beta$ A domain  $\alpha$ 1 helix (residues 128–145). This contact is shown in Fig. 2 C (top and middle) and described in more detail in the section entitled An FnIII<sub>10</sub>– $\alpha$ 1 helix contact promotes spontaneous hinge opening.

#### The helical structure of the $\beta$ 1– $\alpha$ 1 loop is restored

Between the unliganded  $\alpha$ , $\beta_3$  and the liganded  $\alpha_{IIb}$ , $\beta_3$  integrin crystal structures, a single turn of the 3<sub>10</sub> helix in the  $\beta$ A domain

$\beta$ 1– $\alpha$ 1 loop (residues 121 to 127) is moved inward en bloc, and a bend between this region and the  $\alpha$ 1 helix is straightened, such that the  $\beta$ 1– $\alpha$ 1 loop and  $\alpha$ 1 helix are joined into one continuous helix (Xiong et al., 2001; Xiao et al., 2004). In both of these structures, the ADMIDAS ion is directly coordinated by Asp<sup>127</sup>, which is located where the  $\beta$ 1– $\alpha$ 1 loop joins the  $\alpha$ 1 helix. In contrast, the 3<sub>10</sub> helix in the  $\beta$ 1– $\alpha$ 1 loop is disrupted, and Asp<sup>127</sup> does not coordinate the ADMIDAS ion in the liganded  $\alpha$ , $\beta_3$  integrin crystal structure (Xiong et al., 2002). We found that when the coordinates of this structure are minimized for 2,000 steps before equilibration with MD, direct contact between Asp<sup>127</sup> and the ADMIDAS ion formed (six out of six times) and the helical structure of the  $\beta$ 1– $\alpha$ 1 loop was restored (Fig. 3, A vs. C–F), regardless of a change in the ADMIDAS ion from Mg<sup>2+</sup> to Ca<sup>2+</sup> (Fig. 3, K–N). At the beginning of MD equilibrations in Mg<sup>2+</sup>-occupied complexes, the  $\alpha$ 1 helix joined together with the  $\beta$ 1– $\alpha$ 1 loop to form one uninterrupted helical structure (Fig. 3, C and D).

#### The MIDAS conformation found in liganded crystal structures promotes hinge opening

In both available crystal structures that contain the ligand-bound  $\beta$ A domain, the distance between the MIDAS ion and the carboxyl oxygens of Asp<sup>119</sup> is  $\sim 4 \text{ \AA}$ . It was suggested that a water molecule likely bridged this distance in the  $\alpha$ , $\beta_3$  structure

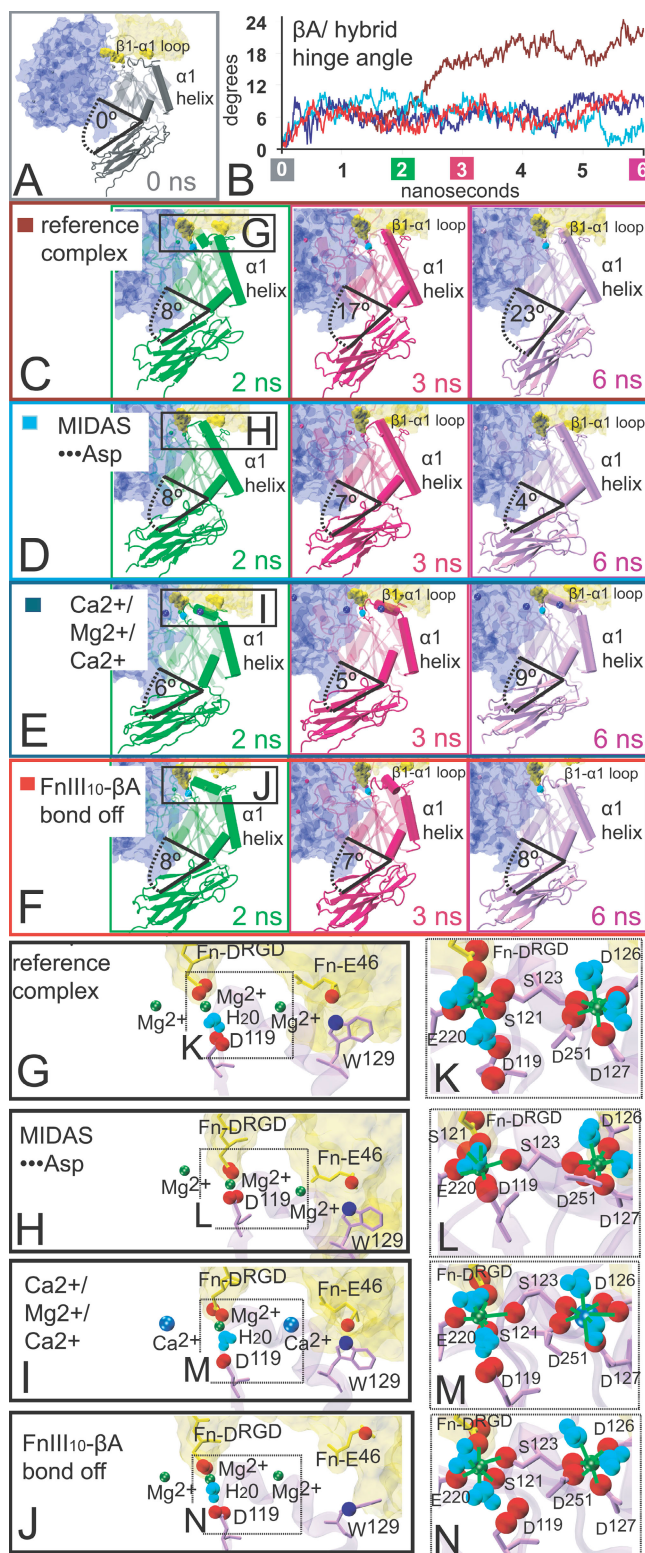


**Figure 3. Minor structural changes perturb the  $\alpha 1$  helix and deter hinge opening.** (A) The starting complex. (B) Hinge angle values traced over time for four separate equilibrations of the integrin complex. (C–F) Snapshots corresponding to each of these four equilibrations are shown with the hinge-angle values indicated. Only in the reference complex (C) did the hinge angle increase by  $\sim 20^\circ$ . When, instead, the  $\alpha 1$  helix was shifted slightly outward as a result of a 2-Å MIDAS shift (D), or was interrupted as a result of  $\text{Ca}^{2+}$  at the ADMIDAS (E) or instability of the E<sup>46</sup>-W<sup>129</sup> bond (F), the hinge did not significantly increase in the same 6-ns

and, indeed, in the  $\alpha_{IIb}\beta_3$  structure that was resolved at a higher resolution, a water molecule was found to be present between Asp<sup>119</sup> and the MIDAS ion. In two out of three separate equilibrations that we initially performed on the  $\alpha_v\beta_3$ -FnIII<sub>10</sub> complex, ranging from 1 to 8 ns, a water molecule diffused into this location between the MIDAS ion and Asp<sup>119</sup> early on and remained there. In subsequent equilibrations, we placed a water molecule there manually. In 17 separate equilibrations (1 ns each; unpublished data), we found that this water molecule either remained between the ion and Asp<sup>119</sup> (nine times) or diffused away (eight times).

When the water diffused away, the MIDAS ion shifted  $\sim 2$  Å into direct contact with Asp<sup>119</sup>. Because the two different MIDAS conformations obtained in this study are thus distinguished by their Asp<sup>119</sup> contact, we refer hereafter to the original MIDAS conformation resolved in crystal structures and maintained in the reference complex that was previously described as “MIDAS- $\cdots \text{H}_2\text{O} \cdots$  Asp” (Fig. 3, K, M, and N), and to the shifted MIDAS conformation as “MIDAS-Asp” (Fig. 3 L). For a comparison between these two  $\beta A$  domain MIDAS conformations and the two  $\alpha A$  domain MIDAS conformations that were previously established (Lee et al., 1995), see Fig. S2 (available at <http://www.jcb.org/cgi/content/full/jcb.200602071/DC1>).

Aside from differences in Asp<sup>119</sup> contact, all ion-coordinating residues are identical between MIDAS- $\cdots \text{H}_2\text{O} \cdots$  Asp and MIDAS-Asp complexes. In other words, all residues other than Asp<sup>119</sup> that directly coordinate the MIDAS, LIMBS, or ADMIDAS ions remained the same in the presence of both MIDAS conformations (Fig. 3, K and N vs. L).

Over the first 2.5 ns of every equilibration that we performed, both unliganded and liganded and independent of the 2-Å MIDAS shift or other structural perturbations, the hinge angle between the  $\beta A$  and hybrid domains increased by  $\sim 6^\circ$ . At this value, the conserved  $\beta A$ /hybrid domain hydrogen bond between Asn<sup>303</sup> and Lys<sup>417</sup> was able to remain formed. When an equilibration containing the MIDAS-Asp conformation was extended to 6 ns, the  $\beta A$ /hybrid hinge increase of this FnIII<sub>10</sub> integrin complex remained at  $6 \pm 2^\circ$ . Thus, we asked how the 2-Å MIDAS shift deters  $\beta A$ /hybrid domain hinge opening.

time window.  $\beta$ -Subunit domains, shown in cartoon representation, are colored by time point. Within the  $\beta A$  domain, the  $\beta 1$ - $\alpha 1$  loop,  $\alpha 1$ , and  $\alpha 7$  helix are emphasized by opaque shading. In each snapshot, the  $\alpha$ -subunit domain and FnIII<sub>10</sub> are shown in transparent surface blue and yellow representations, respectively. (G) Close-up of the  $\beta A$  domain-binding pocket in the reference complex reveals the MIDAS- $\cdots \text{H}_2\text{O} \cdots$  Asp conformation, which is visible by the water molecule (cyan) between the MIDAS ion and Asp<sup>119</sup>; Mg<sup>2+</sup> (green) at the LIMBS, MIDAS, and ADMIDAS; and the FnIII<sub>10</sub>- $\beta A$  domain-binding contact between E<sup>46</sup> and W<sup>129</sup>. (H–J) Close-ups from the three additional equilibrations, corresponding to the snapshots in D–F, respectively, indicate the specific structural alterations that made each complex unique, which were the switch to the MIDAS-Asp conformation (H), Ca<sup>2+</sup> (blue) in place of Mg<sup>2+</sup> at the LIMBS and ADMIDAS (I), and (J) no E<sup>46</sup>-W<sup>129</sup> bond. (K–N) MIDAS- and ADMIDAS-coordinating residues are shown for each complex. These residues are identical in every case except in L, where Asp<sup>119</sup> joined the MIDAS coordination sphere in the switch to the MIDAS-Asp conformation, and in M, where the second oxygen from Asp<sup>126</sup> joined the ADMIDAS coordination in the switch from Ca<sup>2+</sup> to Mg<sup>2+</sup> at this position.

We found that over the first 2.5 ns, the  $\alpha 1$  helix of the MIDAS $\cdots$ Asp complex moved outward relative to its position in the starting crystal structure (Fig. 4 C). In contrast, during the same timeframe of the reference complex equilibration, before the substantial hinge increase that this complex later displayed, the  $\alpha 1$  helix moved inward (Fig. 4, A and B and Video 1).

At the top of the  $\alpha 1$  helix, ADMIDAS ion-coordinating residues Asp<sup>127</sup> and Asp<sup>126</sup> are linked along the  $\beta 1\text{--}\alpha 1$  loop to MIDAS residues Ser<sup>123</sup>, Ser<sup>121</sup>, and Asp<sup>119</sup>. Thus, when the  $\beta 1\text{--}\alpha 1$  loop was repositioned in association with the shift to the MIDAS $\cdots$ Asp conformation, the  $\alpha 1$  helix was repositioned as well (Fig. S3, available at <http://www.jcb.org/cgi/content/full/jcb.200602071/DC1>). Notably, the  $\alpha 1$  helix also contacts the C-terminal  $\alpha 7$  helix and the outside of the  $\beta A$ /hybrid hinge through noncovalent interactions at its middle and bottom, respectively. In this fashion, the MIDAS position of the reference complex promotes an inward “lever-arm” motion of the joined  $\beta 1\text{--}\alpha 1$  loop/ $\alpha 1$  helix; the key to how the MIDAS shift deterred hinge opening was by disruption of this lever-arm mechanism. This finding was reproduced in a second 6-ns MIDAS $\cdots$ Asp equilibration. For further depiction, see Fig. S3.

#### $\text{Ca}^{2+}$ at the ADMIDAS impedes hinge opening

$\text{Ca}^{2+}$  at the ADMIDAS has been shown to inhibit integrin activation (Mould et al., 2002) and mutation of the ADMIDAS Asp residues has been shown to override this effect (Chen et al., 2003). Mutation of the ADMIDAS has also been shown to disrupt the transduction of conformational change between the MIDAS and the  $\beta A$ /hybrid hinge (Mould et al., 2003a). To investigate the impact of  $\text{Ca}^{2+}$  on the conformation of the integrin headpiece complex, we replaced  $\text{Mg}^{2+}$  with  $\text{Ca}^{2+}$  in all ion-binding sites, except for the MIDAS, because occupation of the MIDAS by  $\text{Mg}^{2+}$  is known to be important for ligand binding (Mould et al., 1995, 2002). Hereafter, we shall refer to this ion arrangement as “ $\text{Ca}^{2+}\text{--Mg}^{2+}\text{--Ca}^{2+}$ ,” in reference to the occupancies of the LIMBS, MIDAS, and ADMIDAS, respectively. With  $\text{Ca}^{2+}$  in place of  $\text{Mg}^{2+}$ , the second carboxylate oxygen of the Asp<sup>126</sup> side chain joined the ADMIDAS coordination sphere (Fig. 3 M). This is consistent with crystallographic data of the  $\text{Ca}^{2+}$ -occupied ADMIDAS, in both liganded and unliganded integrin structures (Xiong et al., 2001, 2002; Xiao et al., 2004).

Although the water in the MIDAS $\cdots\text{H}_2\text{O}\cdots$ Asp conformation remained consistently in place (Fig. 3 M) in three out of three separate  $\text{Ca}^{2+}\text{--Mg}^{2+}\text{--Ca}^{2+}$  equilibrations (1 ns each), the  $\beta A$ /hybrid hinge did not increase beyond  $6 \pm 2^\circ$  when one of these equilibrations was extended to 8 ns.

In every  $\text{Ca}^{2+}\text{--Mg}^{2+}\text{--Ca}^{2+}$  equilibration we observed (ranging from 1 to 8 ns), a break between the  $\beta 1\text{--}\alpha 1$  loop and  $\alpha 1$ -helix structure occurred early on, in the vicinity of Asp<sup>126</sup> (Fig. 3, E vs. C and D). In the first 2.5 ns, the  $\beta 1\text{--}\alpha 1$  loop displayed little change from its position in the starting crystal structure, whereas the  $\alpha 1$  helix moved outward (Fig. 4 E and Video 3, available at <http://www.jcb.org/cgi/content/full/jcb.200602071/DC1>). Thus, although the movement of the  $\beta 1\text{--}\alpha 1$  loop resembled that of the reference complex in which

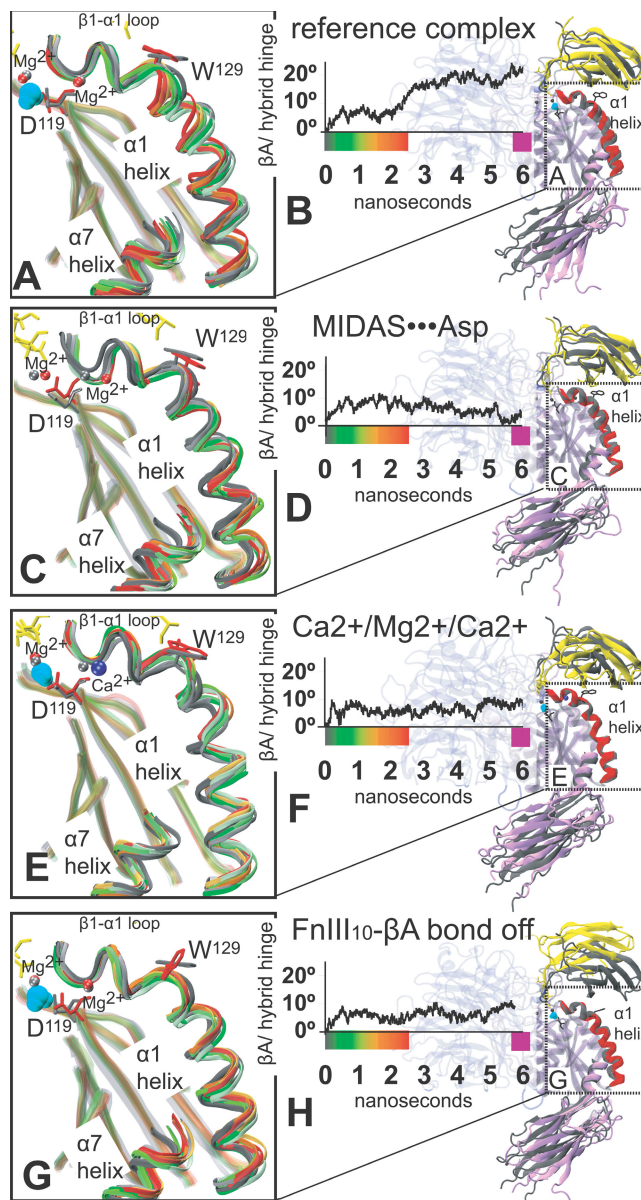


**Figure 4. Hinge opening follows the inward lever-arm movement of the  $\alpha 1$  helix.** In all images, gray, green, red, and purple indicate the conformation at 0, 1, 2.5, and 6 ns, respectively. The MIDAS $\cdots\text{H}_2\text{O}\cdots$ Asp conformation is visible by the water molecule (cyan) located between the MIDAS ion and Asp<sup>119</sup>. (A) 10 snapshots over the first 2.5 ns of the reference equilibration are aligned with the starting crystal structure (PDB code 1L5G) via the  $\beta A$  domain  $\beta$ -strands. The  $\alpha 1$  and  $\alpha 7$  helices are shown and colored according to 250-ps intervals. From gray to red, the path of the  $\alpha 1$  helix is inward and upward. (B) The inward movement of the  $\alpha 1$  helix occurred before a significant jump in the hinge value, as indicated in the trace of the hinge over time and (far right) depicted by alignment with the starting crystal structure of the  $\alpha 1$  helix at 2.5 ns (red) and the  $\alpha 7$  helix and  $\beta A$ /hybrid domain at 6 ns (purple). (C–H) The same pictorial scheme is used to depict the three additional equilibrations in which various structural perturbations (Fig. 3) occurred and hinge opening was hindered. Notably, as evident by the presence of gray inside the  $\alpha 1$ -helix close-ups shown in C, E, and G, the path of the  $\alpha 1$  helix was outward over the first 2.5-ns of these equilibrations. For dynamic, 3D views, see Videos 1–4, available at <http://www.jcb.org/cgi/content/full/jcb.200602071/DC1>.

the hinge increased, the movement of the  $\alpha 1$  helix resembled that of the MIDAS $\cdots$ Asp complex, and just as in that complex, the hinge did not substantially increase (Video 4).

Downloaded from on June 8, 2017

### An FnIII<sub>10-α1</sub> helix contact promotes hinge opening

In all equilibrations of the integrin complex described thus far, a stable hydrogen bond consistently formed between Glu<sup>46</sup>, which is a conserved acidic residue on the same face of FnIII<sub>10</sub> as the RGD sequence, and Trp<sup>129</sup>, which is located at the top of the α1-helix (Fig. 2 C, orange line). In two repeat reference complex equilibrations, this Glu<sup>46</sup>-Trp<sup>129</sup> bond broke at either 1 or 3 ns, and the hinge increase of ~20° either did not occur in the 6-ns time window or occurred but was delayed by ~2 ns relative to the original reference complex, respectively (Fig. S4, available at <http://www.jcb.org/cgi/content/full/jcb.200602071/DC1>). In a third reference complex repeat equilibration, we deliberately disrupted the Glu<sup>46</sup>-Trp<sup>129</sup> bond at 1 ns by turning off the charge of the nitrogen in the Trp<sup>129</sup> side chain. When this computationally “mutated” complex was equilibrated for 5 ns, the α1 helix became distorted (Fig. 3 F) and moved outward (Fig. 4 G), and the hinge angle did not substantially increase (Fig. 4 H). From these studies, we linked the stability of the Glu<sup>46</sup>-Trp<sup>129</sup> contact with an inward movement of the α1 helix early on in the equilibration and with an ~20° hinge-angle increase on a 6-ns timeframe. In other words, we found that, like MIDAS-Asp and Ca<sup>2+</sup>-Mg<sup>2+</sup>-Ca<sup>2+</sup> complexes, the absence of substantial hinge opening in Mg<sup>2+</sup>-occupied complexes was also linked with an outward α1-helix shift (Fig. 3, E and F; and Fig. 4, E and G). Sequence analysis indicates that the Glu<sup>46</sup>-Trp<sup>129</sup>-binding contact is unique to β<sub>3</sub> integrins (Fig. S4).

Traces of the βA/hybrid domain hinge-angle value over time for the aforementioned four distinct integrin complexes are overlaid in Fig. 3 B and shown separately in Fig. 4.

### Comparison to the unliganded α<sub>v</sub>β<sub>3</sub> integrin headpiece

To gain a sense of how these structural snapshots fit along the allosteric pathway of ligand-induced integrin activation, we equilibrated the same headpiece domains from the unliganded α<sub>v</sub>β<sub>3</sub> crystal structure occupied with Mg<sup>2+</sup> (Xiong et al., 2001). The α1 helix of this structure is split in half and this split remained throughout the 6-ns equilibration (Fig. 5 A). Coordination of the ADMIDAS ion by Ser<sup>123</sup> was lost early on, and the β1-α1 loop exhibited a substantially wider range of movement relative to the dynamics of this loop in liganded integrin complexes (Fig. 5 B vs. Fig. 4; and Video 5, available at <http://www.jcb.org/cgi/content/full/jcb.200602071/DC1>), illustrating the stabilizing effect that ligand-binding together with LIMBS and MIDAS occupancy bring to this structural region. Aside from Ser<sup>123</sup>, the starting ADMIDAS coordination remained unchanged, and the βA/hybrid domain hinge varied by 8 ± 3° relative to its starting value. Like the aforementioned integrin complexes, in which the hinge also did not substantially increase, the conserved Asn<sup>303</sup>-Lys<sup>417</sup> hydrogen bond located where the closed hinge is most acute (Fig. 2 B) was still able to form after 6 ns (Video 6).

A comparison across all equilibrations described thus far reveals a higher degree of floppiness at the bottom of the α1 helix in structures in which hinge opening was not observed during the nanosecond time window, as indicated by comparison

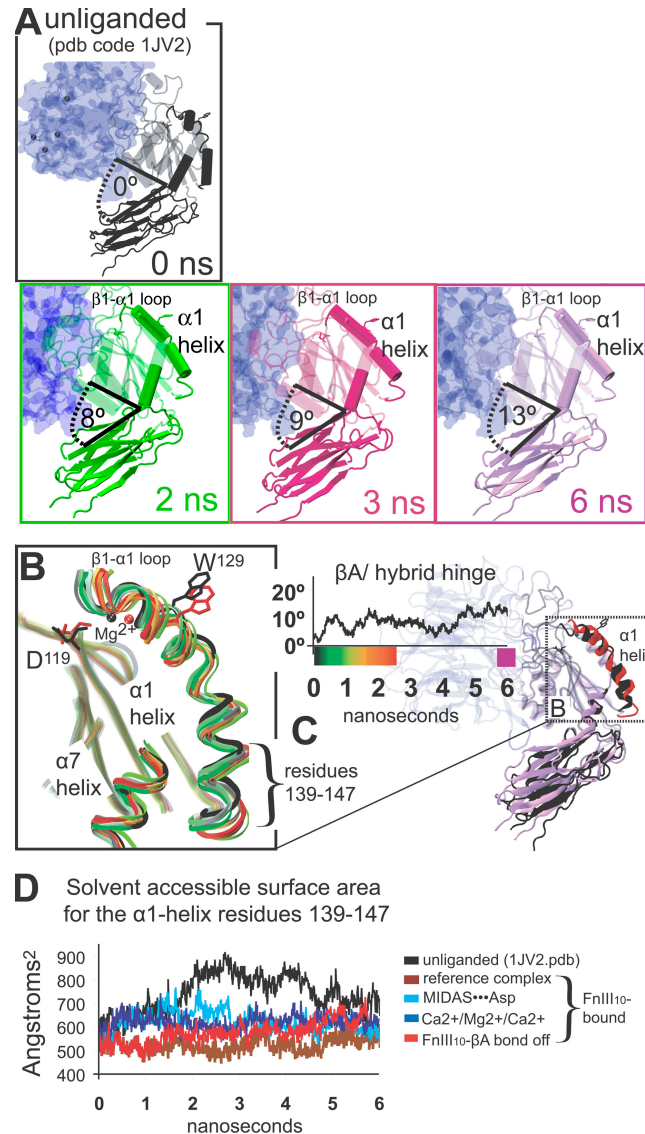


**Figure 5. Significant fluctuations of the α1 helix and β1-α1 loop in the unliganded integrin equilibration.** (A) Snapshots from the equilibration of the unliganded α<sub>v</sub>β<sub>3</sub> integrin headpiece domains (Xiong et al., 2001) are shown in the same pictorial scheme as Fig. 3 (C–F), for comparison. (B) 10 snapshots over the first 2.5 ns of this equilibration are aligned with the starting crystal structure (PDB code 1JV2) via the βA domain β-strands and colored according to 250-ps intervals, as described in Fig. 4. From black to red, significant outward and downward movement of the β1-α1 loop and α1 helix is evident. (C) The hinge angle is traced over time. The equilibrated complex is aligned with the starting crystal structure. Black, red, and purple indicate time points at 0, 2.5, and 6 ns, respectively. (D) The increased solvent-accessible surface area at the bottom of the α1 helix during equilibration of the unliganded integrin domains (black) is compared with that of the four FnIII<sub>10</sub>-bound integrin complexes. For dynamic 3D views, see Videos 5 and 6, available at <http://www.jcb.org/cgi/content/full/jcb.200602071/DC1>.

over time of the average solvent-accessible surface area in this location (residues 139–147; Fig. 5 D). In other words, the bottom of the α1 helix displayed the least fluctuations in the solvent-accessible surface area (indicating structural stability), as well as the least accessibility to water (in agreement with the inward helical shift) in the reference complex in which the hinge opened spontaneously (Fig. 5 D, red line), whereas the same

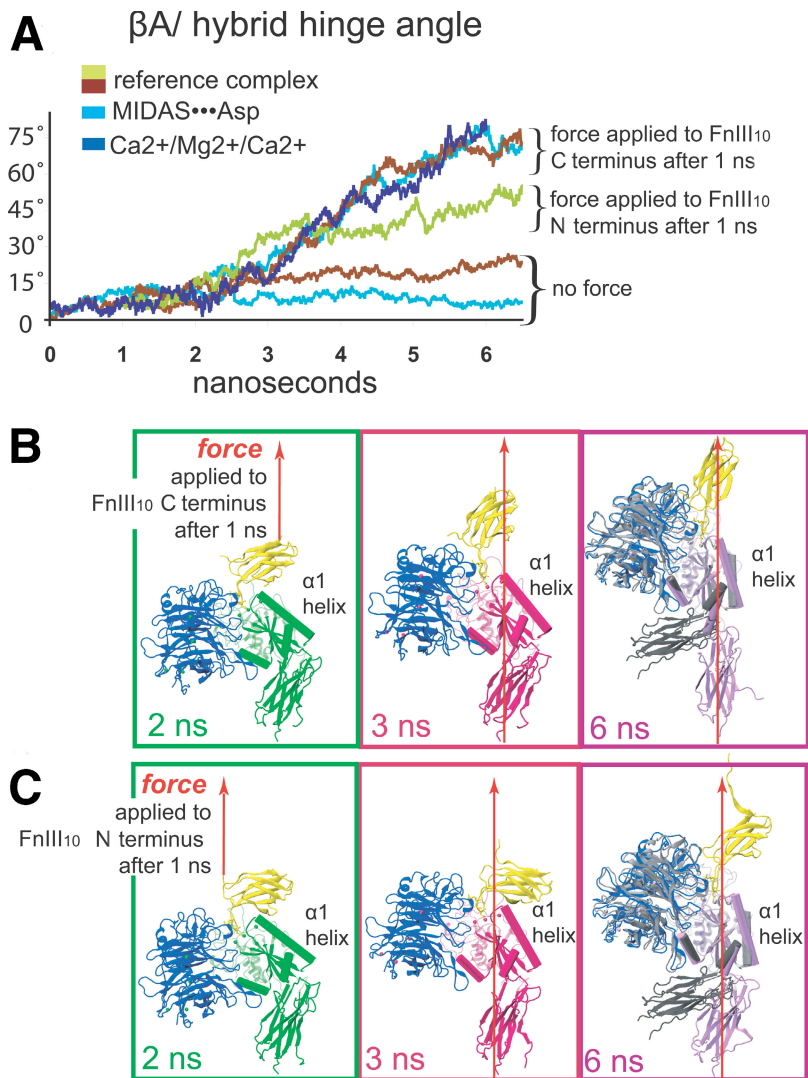


**Figure 6. Mechanical force accelerates hinge opening.** (A) Traces of the change in the hinge angle over time from both MD- and SMD-simulations are overlaid. SMD simulations were begun after complexes were equilibrated for 1 ns. (B) Snapshots from the SMD simulation in which the hinge was opened by ~70° by pulling for 5 ns on the C terminus of FnIII<sub>10</sub> at 10 Å/ns. β-Subunit domains are colored according to time point. For dynamic 3D views, see Videos 7 and 8. (C) Corresponding time points from the SMD simulation in which the hinge angle was opened by ~50° by pulling for 5 ns on the N terminus of FnIII<sub>10</sub> at 10 Å/ns. In the last frame of both C and D, the SMD-derived structures, after 6 ns for each pulling vector (shown with β-subunit domains in purple), are aligned with the starting crystal structure (gray) via the βA domain β-strands. Videos 7 and 8 are available at <http://www.jcb.org/cgi/content/full/jcb.200602071/DC1>.

structural region in the unliganded integrin displayed considerable fluctuations (Fig. 5 D, black line).

#### Mechanical force opens the hinge

To see if the closed hinge could be opened by mechanical force, we applied force between the C-terminal ends of FnIII<sub>10</sub> and the β-hybrid domain after 1 ns of equilibration, at which time the hinge angle was only ~6° greater than its starting value. In a total of seven separate SMD simulations (three of the reference complex, two of the MIDAS...Asp complex, and two of the Ca<sup>2+</sup>-Mg<sup>2+</sup>-Ca<sup>2+</sup> complex), we found that pulling with a constant velocity of 10 Å/ns caused the βA/hybrid domain hinge to increase by ~70° over 5 ns (Fig. 6, A and B; and Videos 7 and 8, available at <http://www.jcb.org/cgi/content/full/jcb.200602071/DC1>). At this value, the βA and hybrid domains were aligned along the vector of force and continued strain did not increase the hinge further.

In two additional SMD simulations, the hinge was increased by ~50° over 5 ns when force was applied to the N-terminal end of FnIII<sub>10</sub> instead (Fig. 6, A and C). In every SMD simulation (nine in total), the hinge increased in the same characteristic fashion, independent of the FnIII<sub>10</sub> terminus to which force was applied

and whether or not FnIII<sub>10</sub> started to unravel under the strain (Fig. S5, available at <http://www.jcb.org/cgi/content/full/jcb.200602071/DC1>). Also, in every case, the principle force-bearing binding contact between Asp<sup>RGD</sup> of FnIII<sub>10</sub> and the MIDAS ion was well maintained. When the force was applied between FnIII<sub>10</sub> and the C terminus of the α-subunit propeller domain instead, the hinge could not be pulled open (unpublished data).

As a control, we deleted FnIII<sub>10</sub> and applied force directly to the MIDAS ion in the reference, MIDAS...Asp, and Ca<sup>2+</sup>-Mg<sup>2+</sup>-Ca<sup>2+</sup> integrin structures. Each time (three out of three), force applied between the MIDAS and the hybrid domain increased the hinge in the same characteristic fashion of ~70° over 3 ns (unpublished data).

Thus, the key finding of these investigations is that the βA/hybrid hinge opens when force is applied between the MIDAS ion and the hybrid domain.

#### Force-induced opening of the hinge reverses α1-helix distortion

We have shown that a characteristic feature of spontaneous βA/hybrid hinge opening is the inward shift of the α1 helix

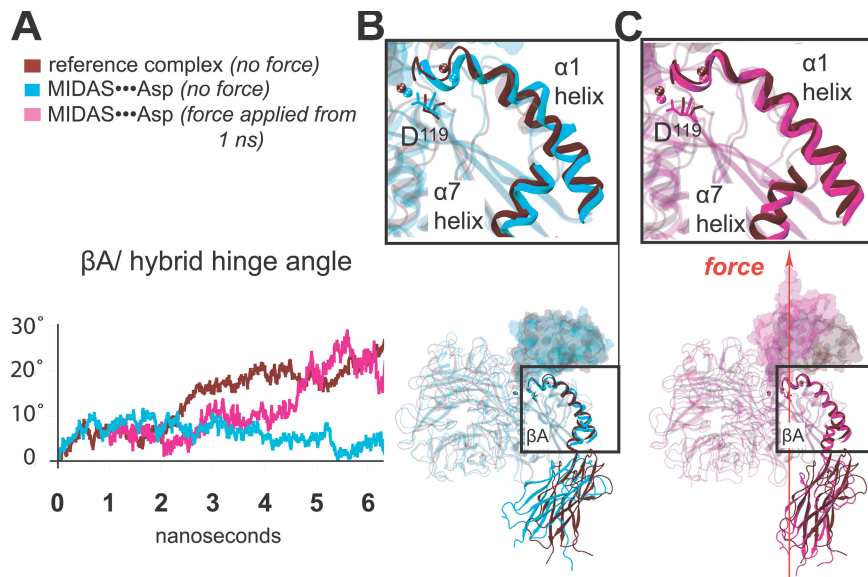
**Figure 7. Force-induced opening of the hinge reverses outward  $\alpha$ 1-helix distortion.** (A) Traces of the hinge angle over time show that although the hinge of the MIDAS...Asp complex did not open under equilibration conditions (cyan), mechanical force induced the hinge angle of this complex to open (pink) by the same amount that was found to occur spontaneously in the MIDAS...H<sub>2</sub>O...Asp complex under equilibration conditions (dark red). (B) The MD-derived MIDAS...Asp and MIDAS...H<sub>2</sub>O...Asp complexes, aligned after 6 ns of equilibration each and shown in cyan and dark red, respectively. The hinge angle difference between these complexes is 21° at this time point. (top) Close-up of the aligned  $\beta$ A domains reveal a difference between the  $\alpha$ 1-helix conformations. The  $\beta$ 1- $\alpha$ 1 loop,  $\alpha$ 7 helix, ions, and Asp<sup>119</sup> of each structure are also shown as opaque, for orientation. (C) The SMD-derived MIDAS...Asp complex (pink) and the MD-derived MIDAS...H<sub>2</sub>O...Asp complex (dark red) are aligned after 6 ns of simulation time each. The hinge angle of each complex is now 21°. (Top) Close-up of the aligned  $\beta$ A domains reveal a new similarity between the  $\alpha$ 1-helix conformations.

(Fig. 4, A and B). This finding is further illustrated in Fig. 7 B by alignment of the reference and MIDAS...Asp integrin complexes after 6 ns of equilibration each. Because the hinge angle of the MIDAS...Asp complex did not increase beyond  $6 \pm 2^\circ$  under equilibration conditions on the nanosecond timescale, we asked if opening the hinge by force would induce the  $\alpha$ 1 helix of this complex to resemble that of the reference complex in which the hinge angle had increased spontaneously.

After 1 ns of equilibration, force was applied to the MIDAS...Asp complex by pulling on the FnIII<sub>10</sub> C terminus with a constant velocity of 5 Å/ns. After 5 ns of pulling, the hinge of this complex was increased by 21°, which is the same hinge value that the reference complex displayed at 6 ns without force (Fig. 7 A). Comparison of the  $\alpha$ 1 helices of these two structures at this time point reveals a striking similarity (Fig. 7 C). Thus, we found that force-induced opening of the  $\beta$ A/hybrid hinge reverses the elastic distortion in the  $\alpha$ 1 helix that occurred when the hinge remained closed.

## Discussion

Integrin activation is known to have a structural origin (Takagi and Springer, 2002; Luo et al., 2005), yet the key sequential details of activating conformational change have been controversial. For example, experiments have shown that ligand binding to the integrin head induces the opening of the hinge between the  $\beta$ A and hybrid headpiece domains (Takagi et al., 2002, 2003; Mould et al., 2003c; Xiao et al., 2004; Iwasaki et al., 2005), but this hinge is closed in the liganded  $\alpha_v\beta_3$  crystal structure (Xiong et al., 2002). We replaced the peptide ligand of this structure with FnIII<sub>10</sub> and revealed in MD simulations of the isolated integrin headpiece complex how ligand-induced structural change propagates across the  $\beta$ A domain via the  $\alpha$ 1 helix, to then be amplified by an increase in the remote  $\beta$ A/hybrid hinge. In separate equilibrations of the same complex, three different structural perturbations at the top of the  $\beta$ A domain induced small, elastic distortions in the  $\alpha$ 1 helix,



and the hinge did not increase substantially in the nanosecond time window. The structural variations that we found to impede hinge opening on the nanosecond timescale are a 2-Å MIDAS shift, Ca<sup>2+</sup> in place of Mg<sup>2+</sup> at the LIMBS and ADMIDAS, and disruption of an FnIII<sub>10</sub>- $\alpha$ 1 helix-binding contact. In equilibration of the unliganded integrin headpiece domains (Xiong et al., 2001), maximum fluctuations of the  $\beta$ 1- $\alpha$ 1 loop and  $\alpha$ 1 helix were found to occur. Together, these investigations enabled us to deduce the allosteric pathway whereby a small inward (vs. outward) movement of the  $\alpha$ 1 helix promotes (or impedes)  $\beta$ A/hybrid domain hinge opening. In addition to predicting a role for a new FnIII<sub>10</sub>- $\beta$ <sub>3</sub> integrin contact located outside of the RGD-binding pocket, these findings offer a structural basis for mAb experimental data that also link an outward  $\alpha$ 1-helix position with Ca<sup>2+</sup> in place of Mg<sup>2+</sup> at the ADMIDAS and an inward  $\alpha$ 1-helix position with hinge opening and integrin activation (Mould et al., 2002, 2003b).

The crystal structures of the unliganded  $\alpha_v\beta_3$ - and the liganded  $\alpha_{IIb}\beta_3$  integrins provide stationary endpoints before and after the transition of the integrin headpiece to the open conformation of the  $\beta$ A/hybrid hinge, respectively (Xiong et al., 2001; Xiao et al., 2004). Together with experiments that have linked integrin activation with  $\beta$ A/hybrid hinge opening (Mould et al., 2003b; Luo et al., 2004b; Iwasaki et al., 2005), we propose that the unliganded  $\alpha_v\beta_3$  structure represents a low-affinity state of the integrin headpiece (which we shall call “state 1”), and the liganded  $\alpha_{IIb}\beta_3$  structure represents a high-affinity state of the integrin headpiece (hereafter referred to as “state 2”). In this framework, the MD-derived conformations presented in this study are snapshots along the ligand-induced transition from state 1 to state 2 (Fig. 8).

Quite unusual for domain-domain contacts,  $\beta$ A connects to the hybrid domain via two peptide linkers, at both the C and N terminus. In this fashion, floppiness of the  $\beta$ A/hybrid hinge itself is greatly restricted. A key finding of this study is the allosteric link between floppiness and distortion in the  $\beta$ A domain  $\alpha$ 1 helix and the opening of the  $\beta$ A/hybrid hinge. Although we

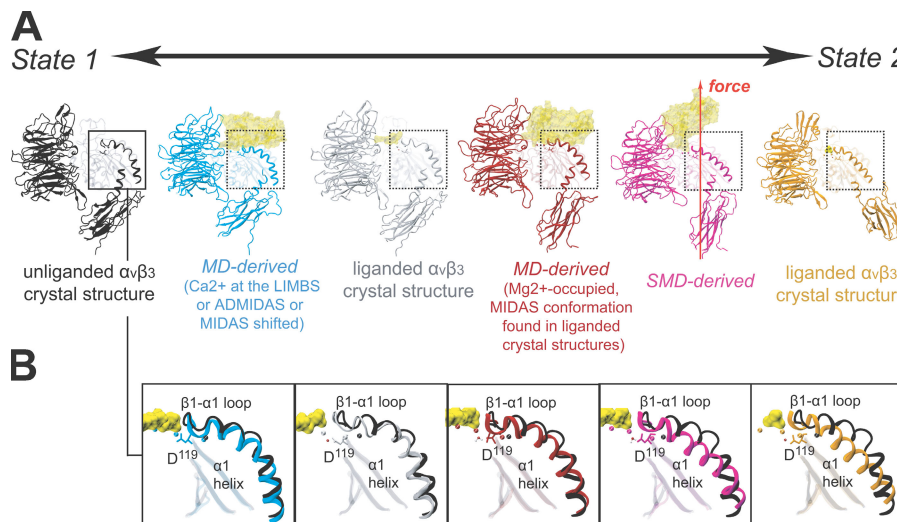


**Figure 8. Transitional snapshots along the hinge-opening pathway.** (A) The unliganded  $\alpha_v\beta_3$ , liganded  $\alpha_v\beta_3$ , and liganded  $\alpha_{IIb}\beta_3$  integrin crystal structures are shown in black, gray, and orange, respectively (Xiong et al., 2001, 2002; Xiao et al., 2004). A representative MD-derived snapshot, in which a structural perturbation hindered hinge angle opening, is indicated in blue. The MD-derived snapshot in which the hinge angle increased spontaneously is indicated in dark red. The SMD-derived snapshot in which the hinge angle was increased by mechanical force is shown in pink. (B) Close-ups of  $\beta$ A domain  $\alpha 1$  helices for each structural snapshot are shown overlaid with the  $\alpha 1$  helix of the unliganded  $\alpha_v\beta_3$  integrin crystal structure (which is proposed to represent state 1). MIDAS and ADMIDAS ions are visible in each close-up.

found that  $\text{Ca}^{2+}$  in place of  $\text{Mg}^{2+}$  at the LIMBS and ADMIDAS resulted in the outward shift of the  $\alpha 1$  helix and no substantial hinge-angle increase on the nanosecond timeframe, experiments have shown that ligand-induced opening of the hinge does ultimately result in  $\text{Ca}^{2+}$  in the LIMBS and ADMIDAS (Xiao et al., 2004). Importantly, although experimental results were obtained under equilibrium conditions in which the strain built-up by ligand binding had sufficient time to be released by the opening of the  $\beta$ A/hybrid hinge, the nonequilibrium snapshots described in this study probe structural dynamics on the nanosecond timescale and, thus, reveal how the ligand-induced strain either propagates to the  $\beta$ A/hybrid interface and is released by hinge-angle opening or, as a result of conformational variations near the binding site, produces elastic  $\alpha 1$ -helix distortions. Notably, the liganded  $\alpha_{IIb}\beta_3$  integrin crystal structure, which presents the open-hinge conformation with  $\text{Ca}^{2+}$  at the LIMBS and ADMIDAS, also displays the inward-shifted  $\alpha 1$  helix joined together with the  $\beta 1-\alpha 1$  loop, which is not found in integrin crystal structures with closed  $\beta$ A/hybrid hinges (Xiong et al., 2001, 2002). Also unique to the  $\alpha_{IIb}\beta_3$  crystal structure is a molecule of glycerol bound directly to the ADMIDAS ion at the top of the  $\alpha 1$  helix (Xiao et al., 2004), which may lend additional stability to this key regulatory region.

These findings address a long-standing debate regarding a feature of the liganded  $\alpha_v\beta_3$ -integrin crystal structure that surprised the integrin community; a severe bend in the legs (Fig. 1 A). Because the structure is liganded, it has been considered to be in the active conformation (Xiong et al., 2002, 2003). However, because the structure was obtained by soaking RGD peptides into unliganded integrin crystals that were preformed with bent legs and closed hinges (Xiong et al., 2002), it has been suggested that the conformation of this structure is the result of constraint imposed by the preexisting crystal lattice (Liddington, 2002; Takagi et al., 2002; Mould et al., 2003b). In support of the latter notion, the legless, liganded  $\alpha_{IIb}\beta_3$  crystal structure, which presents the same MIDAS $\cdots\text{H}_2\text{O}\cdots$ Asp conformation as the liganded  $\alpha_v\beta_3$ -integrin crystal structure, but was formed by cocrystallization with a ligand, displays the open hinge (Xiao et al., 2004). We have shown that once the conformational con-

straints of the leg domains are lifted, the  $\alpha 1$  helix joins together with the  $\beta 1-\alpha 1$  loop and moves inward, and the hinge opens spontaneously on the 6-ns timeframe when the liganded  $\alpha_v\beta_3$  integrin crystal structure is occupied with  $\text{Mg}^{2+}$  and equilibrated in complex with FnIII<sub>10</sub>. Thus, the liganded  $\alpha_v\beta_3$  crystal structure may depict a nonequilibrium headpiece conformation that was constrained along the transition from state 1 to state 2 at a point after RGD peptide-binding had induced a change in the ADMIDAS and  $\beta 1-\alpha 1$  loop and before the strain built-up by this structural perturbation could be relieved by the opening of the  $\beta$ A/hybrid hinge (Fig. S1).

Although the bend in the integrin legs is known to be physiologically relevant (Takagi et al., 2002; Adair et al., 2005), the function of the bend during activation is debated. Currently, two models are widespread; in the “deadbolt” model, activation results from the loss of a constraining contact between the  $\beta$ -tail and  $\beta$ A domains (Xiong et al., 2003), whereas in the “switchblade” model, activation results from extension and separation of the legs and the opening of the  $\beta$ A/hybrid hinge (Takagi and Springer, 2002). Because the legs remain bent in the former and become extended in the latter, these models are often presented as incongruent. However, in both paradigms, the conformation with the bent legs and the closed headpiece hinge angle is low affinity (state 1), and activation necessitates disruption of headpiece-tailpiece contacts. Mutational and mAb experiments have shown that the low-affinity state is stabilized by a close association between the  $\alpha$  and  $\beta$  cytoplasmic tails (Hughes et al., 1995; Kim et al., 2003),  $\alpha$  and  $\beta$  transmembrane helical packing (Luo et al., 2004a, 2005; Partridge et al., 2005), and a close association in multiple points along the  $\alpha$  and  $\beta$  legs (Beglova et al., 2002; Xie et al., 2004; Clark et al., 2005; Mould et al., 2005). According to the switchblade model,  $\alpha$ - and  $\beta$ -subunit contacts stabilize the low-affinity state by constraining the integrin legs in the bent conformation. Recently, electron microscopy studies of the intact, Fn-bound  $\alpha_v\beta_3$  integrin ectodomain were found to display the bent-leg conformation together with a  $\beta$ A/hybrid hinge angle increase of  $\sim 11 \pm 4^\circ$ , relative to the  $\alpha_v\beta_3$  crystal structures (Adair et al., 2005). We have linked an inward shift of the  $\alpha 1$  helix with a hinge increase of  $\sim 20^\circ$  (Fig. 7), indicating

that hinge opening by this amount might already be sufficient to induce affinity-regulating conformational change. Aside from the findings by Adair et al. (2005), studies correlating movement in the headpiece hinge with changes in affinity have been done on integrin ectodomains with modified, truncated, or entirely absent legs (Takagi et al., 2002, 2003; Mould et al., 2003c; Xiao et al., 2004). In consideration of these experimental findings, together with our computational snapshots, we propose that the major physiological role of the bent-leg conformation is to tune, via domain–domain contacts, the height of the energy barrier that has to be overcome for the  $\beta$ A/hybrid hinge to increase and thereby transition the integrin head to the high-affinity state.

Integrin activation is bidirectional and can originate from either the cytoplasmic or the extracellular end of the molecule (Hynes, 2002). The transition of integrins from the low- (state 1) to the high-affinity state (state 2) before ligand binding has been referred to as “priming” (Humphries et al., 2003). When induced from inside the cell, the structural mechanisms underlying priming have been shown to be generated by conformational change in the cytoplasmic tails, transmembrane helices, and leg domains (Takagi et al., 2002; Kim et al., 2003; Partridge et al., 2005). However, conformational changes in these structural regions distal to the ligand-binding site are not required when integrin priming is induced extracellularly (Luo et al., 2004a). In other words, extracellular factors that prime integrins, such as  $Mn^{2+}$  ions, conformation-dependent mAbs that map to the integrin headpiece (Mould et al., 2002, 2003b; Clark et al., 2005), and mutations that induce the shortening of the  $\alpha$ 7 helix (Yang et al., 2004) or the opening of the headpiece hinge (Luo et al., 2003) do so by inducing the high-affinity conformation directly. As expected for an allosterically regulated protein, we thus propose that any mechanism which causes the headpiece hinge angle to open can thereby transition the RGD-binding pocket from state 1 to state 2, even in the absence of bound ligand. Hinge opening and the ensuing inward movement of the  $\alpha$ 1 helix would then constitute the final step in integrin priming.

Finally, we asked how mechanical force might impact the transition between state 1 and state 2, and we found in SMD simulations that force greatly accelerated hinge opening. The force-accelerated transition to the open hinge conformation was accompanied by the same inward movement of the  $\alpha$ 1 helix that we found to be characteristic of hinge opening under equilibrium conditions (Fig. 7). This finding implies that force accelerates hinge opening along the same allosteric pathway. Moreover, we have now shown that a 2- $\text{\AA}$  MIDAS shift or  $Ca^{2+}$  in place of  $Mg^{2+}$  at the ADMIDAS can prevent spontaneous hinge opening, but does not inhibit force-induced hinge opening on the same nanosecond timescale. This finding implies that these structural perturbations raise the energy barrier and that force acting along the  $\beta$ -subunit domains lowers the energy barrier to transition the ligand-bound integrin headpiece from state 1 to state 2. Considering the high sensitivity to minor structural perturbations that these findings reveal, the way in which point mutations to this region enhance (Chen et al., 2003) or disrupt (Mould et al., 2003a) the allosteric activation pathway remains enigmatic.

Because ample experimental data, together with the MD simulations presented in this work, demonstrate that ligand binding can induce the transition from the closed to the open hinge conformation, what would be the advantage of accelerating this transition with force? Kinetic measurements have shown that the ligand-induced conversion of  $\alpha_{IIb}\beta_3$  integrin extracellular domains to the high-affinity conformation occurs on a timescale of  $\sim 10$  s (Müller et al., 1993; Bednar et al., 1997). Yet turnover rates at the timescale of seconds have been reported for constituents in newly formed adhesion sites, and a recent study shows that cells lose their ability to sense the rigidity of their surrounding Fn matrix when the binding of  $\alpha_v\beta_3$  integrins to Fn is blocked (Jiang et al., 2006). Thus, considering the shortness of the time window during which cells have to form adhesions that can sustain cell-generated tension, and assuming that integrins are in state 1 (i.e., not primed) when they first bind to matrix-exposed ligands, mechanical force could then play a physiologically important role in up-regulating the kinetics by which ligand-bound integrins transition from the low- to the high-affinity state. Do integrins then form catch bonds with their RGD ligands, bonds that are switched from a short-lived, low-affinity state to a long-lived, high-affinity state under mechanical force? A preliminary comparison between the  $\alpha_v\beta_3$  integrin complex investigated in this study and the catch bond characteristics of the bacterial adhesin FimH when bound to mannose reveals striking similarities (Tchesnokova et al., 2006) that will be considered in detail elsewhere (unpublished data).

## Materials and methods

### System setup

The crystal structures of the  $\alpha_v\beta_3$  integrin in complex with an RGD-containing mimetic ligand [Protein Data Bank [PDB] code 1L5G; 3.2  $\text{\AA}$  resolution (Xiong et al., 2002)] and FNIII<sub>10</sub> from the FNIII<sub>7-10</sub> tetramer [PDB code 1FNF; 2.0  $\text{\AA}$  resolution (Leahy et al., 1996)] were adopted to build the FNIII<sub>10- $\alpha_v\beta_3$</sub>  starting structure with the program VMD (Humphrey et al., 1996). First, the RGD tripeptides of the two separate structures were aligned, and then the mimetic ligand from the  $\alpha_v\beta_3$  structure was removed. The resulting protein–protein complex contained slight overlap between the C and D strands of FNIII<sub>10</sub> and the  $\beta$ 6- $\alpha$ 7 loop of the  $\beta$ 1-like domain in the integrin  $\beta_3$  subunit. The steric conflict was readily resolved by fixing the RGD tripeptide and rotating the remainder of the FNIII<sub>10</sub> module around the Cy atom of the Arg<sup>RGD</sup>, away from the integrin. The rotation caused an  $\sim 10^\circ$  decrease in the angle formed by the Ca carbons at the N-terminal end, the Asp<sup>RGD</sup>, and the C-terminal end. The two backbone bonds that connect the RGD sequence to the rest of the FNIII<sub>10</sub> module were lengthened after the rotation, but a short minimization of 600 steps restored these bonds to their normal length. The key RGD–integrin–binding contacts, the bond between the Asp<sup>RGD</sup> and the MIDAS cation and the bidentate salt bridge between the Arg<sup>RGD</sup> and  $\alpha_v$ Asp<sup>218</sup>, were well maintained. However, the salt bridge observed in the crystal structure between the ligand and  $\alpha_v$ Asp<sup>150</sup> was broken when the peptide was replaced by the FNIII<sub>10</sub> module. To reduce the integrin to a size that can be feasibly simulated, we used only the  $\beta$ A and hybrid domains of the  $\beta_3$  integrin subunit, the  $\beta$ -propeller domain of the  $\alpha_v$  integrin subunit. The starting structure was solvated in a  $116 \times 115 \times 122$   $\text{\AA}$  TIP3 (Jorgensen et al., 1983) water box, resulting in 153,570 atoms. The water molecule manually added to the MIDAS conformation, between Asp<sup>119</sup> and the MIDAS cation, was placed according to the location of the water molecule in the  $\alpha_{IIb}\beta_3$  integrin crystal structure (Xiao et al., 2004). Seven cations resolved in the headpiece, three resolved in the MIDAS-, LIMBS-, and ADMIDAS-binding pocket motifs, and four resolved in the solvent-exposed  $\beta$  hairpin loops at the bottom of the  $\alpha$ -propeller, were occupied by  $Mn^{2+}$  in the original  $\alpha_v\beta_3$  structure and by  $Mg^{2+}$  in these simulations. For comparison, a solvated complex was also built, in which  $Mg^{2+}$  occupied the MIDAS and  $Ca^{2+}$  occupied the other six ion binding sites. This complex is called

$\text{Ca}^{2+}$ – $\text{Mg}^{2+}$ – $\text{Ca}^{2+}$  in the text, in reference to the occupancies of the LIMBS, MIDAS, and ADMIDAS, respectively.

### Simulation procedure and parameters

All MD simulations were performed with the program NAMD (Phillips et al., 2005) using the CHARMM27 force fields (MacKerell et al., 1998). The system was first minimized for three consecutive 2,000-conjugate gradient steps, during which the protein was initially held fixed and water molecules were allowed to move; next, only the protein backbone was held fixed, and finally, all atoms were allowed to move. After the minimizations, the system was heated from 0 to 300 K in 10 ps and subsequently equilibrated under constant pressure and temperature conditions (NPT). The bidentate salt bridge between Arg<sup>RGD</sup> and Asp<sup>218</sup> of the integrin  $\alpha_v$  domain was held with harmonic constraints until 10 ps into the equilibration and remained stable in all equilibrated structures (Fig. 2 C). A more detailed explanation of the simulation protocol is described elsewhere (Craig et al., 2004). During equilibrations the complex remained stable, exhibiting an overall  $\text{C}\alpha$  RMSD in the head domains (the  $\beta$ -propeller from the  $\alpha_v$  subunit and  $\beta\alpha$  domain from the  $\beta_3$  subunit) of <2.0 Å.

To open the closed hinge under force external forces were applied by SMD protocols at a constant pulling velocity of 5 and 10 Å/ns (Isralewitz et al., 2001). The spring constant was set to 6 kcal/mol/Å<sup>2</sup>. To examine the mechanical response of the complex in various pulling geometries, we fixed either one or both of the  $\text{C}\alpha$  atoms of at the C-terminal residues of the integrin headpiece ( $\alpha_v$ -Arg<sup>438</sup> and/or  $\beta_3$ -Asp<sup>434</sup>) and attached the spring to a  $\text{C}\alpha$  atom at either terminal residue of FnIII<sub>10</sub> (Val<sup>1</sup> or Thr<sup>93</sup>). Generally, the direction of stretching force was chosen along the vector pointing from the fixed atom to the pulling atom. In the special case when both C-terminal ends of the  $\alpha$  and  $\beta$  subunit were fixed, the direction of force was pointed from the midpoint of the two fixed atoms to the pulling atom.

Simulations presented in this work lasted 107 ns altogether. Simulations were completed at the National Center for Supercomputing Applications at the University of Illinois and on the Gonzales cluster at the Swiss Federal Institute of Technology. 1-ns simulation required ~12 h on 128 nodes (IBM) with 1.5-GHz processors (Itanium; Intel), or 24 h on 64 Dlco nodes with 2.4-GHz processors (Opteron; AMD), respectively. All structure alignments were done in VMD (Humphrey et al., 1996) via the backbone atoms of the 6  $\beta\alpha$  domain  $\beta$ -strands (unless otherwise noted). Hinge angles were measured using Hingefind (Wriggers and Schulten, 1997). Figures were rendered using VMD.

### Online supplemental material

Fig. S1 shows the headpiece domains of the liganded  $\alpha_v\beta_3$  integrin structure (1L5G.pdb) aligned with those of the unliganded  $\alpha_v\beta_3$  integrin structure via the backbone atoms of the 6  $\beta\alpha$  domain  $\beta$ -strands. Fig. S2 compares the two previously established conformations of the  $\alpha$  domain MIDAS with the two  $\beta\alpha$  domain MIDAS conformations presented in this study. Fig. S3 depicts the “lever-arm” scenario, in which a 2-Å MIDAS shift causes a characteristic repositioning of the ADMIDAS,  $\beta_1$ - $\alpha_1$  loop, and  $\alpha_1$  helix that we found to impede hinge angle opening. Fig. S4 considers the FnIII<sub>10</sub>- $\beta\alpha$  domain contact between Glu<sup>46</sup> and Tyr<sup>129</sup>, together with additional data and sequence analysis. Within the additional data is a repeat equilibration in which Mg<sup>2+</sup> occupied all binding sites, the MIDAS–H<sub>2</sub>O–Asp conformation was maintained, and the hinge angle again spontaneously increased by ~20°. Fig. S5 describes FnIII<sub>10</sub> domain deformation under force. Videos 1, 3, and 5 show trajectories from the equilibrations of the reference complex, the  $\text{Ca}^{2+}$ – $\text{Mg}^{2+}$ – $\text{Ca}^{2+}$  complex, and the unliganded integrin, respectively. In each case, the MD complex is overlaid with the starting crystal structure. Videos 2, 4, and 6 are 180° rotations around the y axis of the final frames from Videos 1, 3, and 5, respectively. Videos 7 and 8 are the trajectory and the 180° rotation, respectively, of the SMD simulation in which the hinge was opened 70° under force. Online supplemental material is available at <http://www.jcb.org/cgi/content/full/jcb.200602071/DC1>.

We acknowledge Drs. V. Hytönen and M.L. Smith for helpful discussions and C. Faucher for help with figure preparation.

This work was supported by funding from the Swiss Federal Institute of Technology, the Swiss National Computing Centre, the National Institutes of Health (NIH P41RR05969), the National Science Foundation (MCAP3SO28), and the Large Resource Allocation Committee (LRAC MC935028).

Submitted: 13 February 2006

Accepted: 21 September 2006

## References

- Adair, B., J.-P. Xiong, C. Maddock, S. Goodman, M.A. Arnaout, and M. Yeager. 2005. Three-dimensional EM structure of the ectodomain of integrin  $\alpha_v\beta_3$  in a complex with fibronectin. *J. Cell Biol.* 168:1109–1118.
- Bednar, B., M.E. Cunningham, P.A. McQueney, M.S. Egbertson, B.C. Askew, R.A. Bednar, G.D. Hartman, and R.J. Gould. 1997. Flow cytometric measurement of kinetic and equilibrium binding parameters of arginine-glycine-aspartic acid ligands in binding to glycoprotein IIb/IIIa on platelets. *Cytometry*. 28:58–65.
- Beglova, N., S.C. Blacklow, J. Takagi, and T.A. Springer. 2002. Cysteine-rich module structure reveals a fulcrum for integrin rearrangement upon activation. *Nat. Struct. Biol.* 9:282–287.
- Bershadsky, A.D., N.Q. Balaban, and B. Geiger. 2003. Adhesion-dependent cell mechanosensitivity. *Annu. Rev. Cell Dev. Biol.* 19:677–695.
- Calzada, M.J., M.V. Alvarez, and J. Gonzalez-Rodriguez. 2002. Agonist-specific structural rearrangements of integrin alpha IIb beta 3. Confirmation of the bent conformation in platelets at rest and after activation. *J. Biol. Chem.* 277:39899–39908.
- Chen, J., A. Salas, and T.A. Springer. 2003. Bistable regulation of integrin adhesiveness by a bipolar metal ion cluster. *Nat. Struct. Biol.* 10:995–1001.
- Clark, K., R. Pankov, M.A. Travis, J.A. Askari, A.P. Mould, S.E. Craig, P. Newham, K.M. Yamada, and M.J. Humphries. 2005. A specific alpha5beta1-integrin conformation promotes directional integrin translocation and fibronectin matrix formation. *J. Cell Sci.* 118:291–300.
- Copie, V., Y. Tomita, S.K. Akiyama, S. Aota, K.M. Yamada, R.M. Venable, R.W. Pastor, S. Krueger, and D.A. Torchia. 1998. Solution structure and dynamics of linked cell attachment modules of mouse fibronectin containing the RGD and synergy regions: comparison with the human fibronectin crystal structure. *J. Mol. Biol.* 277:663–682.
- Craig, D., M. Gao, K. Schulten, and V. Vogel. 2004. Structural insights into how divalent ions stabilize integrin binding of an RGD peptide under force. *Structure*. 12:2049–2058.
- Hughes, P.E., T.E. O'Toole, J. Ylanne, S.J. Shattil, and M.H. Ginsberg. 1995. The conserved membrane-proximal region of an integrin cytoplasmic domain specifies ligand binding affinity. *J. Biol. Chem.* 270:12411–12417.
- Humphrey, W., A. Dalke, and K. Schulten. 1996. VMD - Visual Molecular Dynamics. *J. Mol. Graph.* 14:33–38.
- Humphries, M.J., P.A. McEwan, S.J. Barton, P.A. Buckley, J. Bella, and A.P. Mould. 2003. Integrin structure: heady advances in ligand binding, but activation still makes the knees wobble. *Trends Biochem. Sci.* 28:313–320.
- Hynes, R.O. 2002. Integrins: bidirectional, allosteric signaling machines. *Cell*. 110:673–687.
- Ingber, D.E. 2003. Mechanobiology and diseases of mechanotransduction. *Ann. Med.* 35:564–577.
- Isralewitz, B., M. Gao, and K. Schulten. 2001. Steered molecular dynamics and mechanical functions of proteins. *Curr. Opin. Struct. Biol.* 11:224–230.
- Iwasaki, K., K. Mitsuoka, Y. Fujiyoshi, Y. Fujisawa, M. Kikuchi, K. Sekiguchi, and T. Yamada. 2005. Electron tomography reveals diverse conformations of integrin alphaIIbbeta3 in the active state. *J. Struct. Biol.* 150:259–267.
- Jiang, G., A.H. Huang, Y. Cai, M. Tanase, and M.P. Sheetz. 2006. Rigidity sensing at the leading edge through alphavbeta3 integrins and RPTPalpha. *Biophys. J.* 90:1804–1809.
- Jorgensen, W.L., J. Chandrasekhar, J.D. Madura, R.W. Impey, and M.L. Klein. 1983. Comparison of simple potential functions for simulating water. *J. Chem. Phys.* 79:926–935.
- Katsumi, A., A.W. Orr, E. Tzima, and M.A. Schwartz. 2004. Integrins in mechanotransduction. *J. Biol. Chem.* 279:12001–12004.
- Kim, M., C.V. Carman, and T.A. Springer. 2003. Bidirectional transmembrane signaling by cytoplasmic domain separation in integrins. *Science*. 301:1720–1725.
- Leahy, D.J., I. Aukhil, and H.P. Erickson. 1996. 2.0 Å crystal structure of a four-domain segment of human fibronectin encompassing the RGD loop and synergy region. *Cell*. 84:155–164.
- Lee, J.O., L.A. Bankston, M.A. Arnaout, and R.C. Liddington. 1995. Two conformations of the integrin A-domain (I-domain): a pathway for activation? *Structure*. 3:1333–1340.
- Liddington, R.C. 2002. Will the real integrin please stand up? *Structure*. 10:605–607.
- Luo, B.-H., T.A. Springer, and J. Takagi. 2003. Stabilizing the open conformation of the integrin headpiece with a glycan wedge increases affinity for ligand. *Proc. Natl. Acad. Sci. USA*. 100:2403–2408.
- Luo, B.-H., T.A. Springer, and J. Takagi. 2004a. A specific interface between integrin transmembrane helices and affinity for ligand. *PLoS Biol.* 2:e153.

- Luo, B.H., K. Strokovich, T. Walz, T.A. Springer, and J. Takagi. 2004b. Allosteric beta1 integrin antibodies that stabilize the low affinity state by preventing the swing-out of the hybrid domain. *J. Biol. Chem.* 279:27466–27471.
- Luo, B.H., C.V. Carman, J. Takagi, and T.A. Springer. 2005. Disrupting integrin transmembrane domain heterodimerization increases ligand binding affinity, not valency or clustering. *Proc. Natl. Acad. Sci. USA.* 102:3679–3684.
- MacKerell, A.D., D. Bashford, M. Bellott, R.L. Dunbrack, J.D. Evanseck, M.J. Field, S. Fischer, J. Gao, H. Guo, S. Ha, et al. 1998. All-atom empirical potential for molecular modeling and dynamics studies of proteins. *J. Physiol. Chem. B.* 102:3586–3616.
- Marinelli, L., A. Lavecchia, K.-E. Gottschalk, E. Novellino, and H. Kessler. 2003. Docking studies on alphavbeta3 integrin ligands: pharmacophore refinement and implications for drug design. *J. Med. Chem.* 46:4393–4404.
- Mould, A.P., S.K. Akiyama, and M.J. Humphries. 1995. Regulation of integrin alpha 5 beta 1-fibronectin interactions by divalent cations. Evidence for distinct classes of binding sites for Mn<sup>2+</sup>, Mg<sup>2+</sup>, and Ca<sup>2+</sup>. *J. Biol. Chem.* 270:26270–26277.
- Mould, A.P., J. Askari, S.J. Barton, A.D. Kline, P.A. McEwan, S.E. Craig, and M.J. Humphries. 2002. Integrin activation involves a conformational change in the alpha-1 helix of the beta-subunit A-domain. *J. Biol. Chem.* 277:19800–19805.
- Mould, A.P., S. Barton, J. Askari, S. Craig, and M.J. Humphries. 2003a. Role of ADMIDAS Cation-binding site in ligand recognition by integrin alpha 5 beta 1. *J. Biol. Chem.* 278:51622–51629.
- Mould, A.P., S.J. Barton, J.A. Askari, P.A. McEwan, P.A. Buckley, S.E. Craig, and M.J. Humphries. 2003b. Conformational changes in the integrin betaA domain provide a mechanism for signal transduction via hybrid domain movement. *J. Biol. Chem.* 278:17028–17035.
- Mould, A.P., E.J. Symonds, P.A. Buckley, J.G. Grossmann, P.A. McEwan, S.J. Barton, J.A. Askari, S.E. Craig, J. Bella, and M.J. Humphries. 2003c. Structure of an integrin-ligand complex deduced from solution x-ray scattering and site-directed mutagenesis. *J. Biol. Chem.* 278:39993–39999.
- Mould, A.P., M.A. Travis, S.J. Barton, J.A. Hamilton, J.A. Askari, S.E. Craig, P.R. Macdonald, R.A. Kammerer, P.A. Buckley, and M.J. Humphries. 2005. Evidence that monoclonal antibodies directed against the integrin beta subunit plexin/semaphorin/integrin domain stimulate function by inducing receptor extension. *J. Biol. Chem.* 280:4238–4246.
- Müller, B., H.-G. Zerwes, K. Tangemann, J. Peter, and J. Engel. 1993. Two step binding mechanism of fibrinogen to alpha IIb beta3 integrin reconstituted into planar lipid bilayers. *J. Biol. Chem.* 268:6800–6808.
- Partridge, A.W., S. Liu, S. Kim, J.U. Bowie, and M.H. Ginsberg. 2005. Transmembrane domain helix packing stabilizes integrin alphaIIbbeta3 in the low affinity state. *J. Biol. Chem.* 280:7294–7300.
- Phillips, J.C., R. Braun, W. Wang, J. Gumbart, E. Tajkhorshid, E. Villa, C. Chipot, R.D. Skeel, L. Kale, K. Schulten. 2005. Scalable molecular dynamics with NAMD. *J. Comput. Chem.* 26:1781–1802.
- Takagi, J., and T.A. Springer. 2002. Integrin activation and structural rearrangement. *Immunol. Rev.* 186:141–163.
- Takagi, J., B.M. Petre, T. Walz, and T.A. Springer. 2002. Global conformational rearrangements in integrin extracellular domains in outside-in and inside-out signaling. *Cell.* 110:599–611.
- Takagi, J., K. Strokovich, T.A. Springer, and T. Walz. 2003. Structure of integrin alpha5beta1 in complex with fibronectin. *EMBO J.* 22:4607–4615.
- Tchesnokova, V., P. Aprikian, O. Yakovenko, B. Kidd, V. Vogel, W.E. Thomas, and E. Sokurenko. 2006. Catch Bond-Mediating FimH Adhesin of *E. coli* is a One-Ligand Allosteric. *Protein.* In press.
- Vogel, V., and M. Sheetz. 2006. Local force and geometry sensing regulate cell functions. *Nat. Rev. Mol. Cell Biol.* 7:265–275.
- Wriggers, W., and K. Schulten. 1997. Protein domain movements: detection of rigid domains and visualization of hinges in comparisons of atomic coordinates. *Proteins.* 29:1–14.
- Xiao, T., J. Takagi, B.S. Collier, J.H. Wang, and T.A. Springer. 2004. Structural basis for allostery in integrins and binding to fibrinogen-mimetic therapeutics. *Nature.* 432:59–67.
- Xie, C., M. Shimaoka, T. Xiao, P. Schwab, L.B. Klickstein, and T.A. Springer. 2004. The integrin alpha-subunit leg extends at a Ca<sup>2+</sup>-dependent epitope in the thigh/genu interface upon activation. *Proc. Natl. Acad. Sci. USA.* 101:15422–15427.
- Xiong, J.-P., T. Stehle, R. Zhang, A. Joachimiak, M. Frech, S.L. Goodman, and M.A. Arnaout. 2001. Crystal structure of the extracellular segment of integrin alpha Vbeta 3. *Science.* 294:339–345.
- Xiong, J.-P., T. Stehle, R. Zhang, A. Joachimiak, M. Frech, S.L. Goodman, and M.A. Arnaout. 2002. Crystal structure of the extracellular segment of integrin alpha Vbeta 3 in complex with an Arg-Gly-Asp ligand. *Science.* 296:151–155.
- Xiong, J.-P., T. Stehle, S. Goodman, and A.M. Arnaout. 2003. New insights into the structural basis of integrin activation. *Blood.* 102:1155–1159.
- Yang, W., M. Shimaoka, J.-F. Chen, and T.A. Springer. 2004. Activation of integrin beta-subunit I-like domains by one-turn C-terminal alpha-helix deletions. *Proc. Natl. Acad. Sci. USA.* 101:2333–2338.